

Evaluation and projection of the annual maximum streamflow in response to anthropogenic and climatic effects under nonstationary conditions in the Hanjiang River Basin, China

Wenlong Hao ^{a,b,*}, Quanxi Shao ^c, Peng Weij^a, Changjun Zhu^a, Xi Chen^d and Rongbo Chen^e

^a College of Energy and Environmental Engineering, Hebei University of Engineering, Handan 056038, China

^b State Key Laboratory of Hydrology-Water Resources and Hydraulic Engineering, Hohai University, Nanjing 210024, China

^c CSIRO Data61, Australian Resources Research Centre, Bentley, WA 6102, Australia

^d Bureau of Hydrology, Changjiang Water Resources Commission, Wuhan 430014, China

^e Power China Kunming Limited, Kunming 650051, China

*Corresponding author. E-mail: hwl5022202@163.com

 WH, 0000-0002-8722-6197; QS, 0000-0002-9768-137X

ABSTRACT

The flood regimes have been changing due to the climate change and human activities. Evaluating the flood risk under nonstationarity is critical to water resource management authorities in disaster reduction. In this study, the annual maximum streamflow (AMS) was used to analyze the nonstationarity in flood frequency in the Hanjiang River (HJR) Basin. A Generalized Additive Model for Location, Scale and Shape (GAMLSS) is employed to characterize nonstationarity in the AMS with time, as well as climatic and anthropogenic factors. Additionally, changes of the AMS in response to future climate change and human activity are also investigated. Results indicate that flood behavior can be better described by the nonstationary model with physically based covariates than that with time and the stationary model, implying that flood regimes of the HJR Basin are mainly influenced by anthropogenic and climatic factors including reservoir, precipitation and temperature. The precipitation and temperature projected by the Statistical Downscaling Model (SDSM) under two climate scenarios (RCP2.6 and RCP4.5) in the HJR Basin are characterized by an increasing trend over the period of 2006–2100. Furthermore, an increasing trend was found in the AMS during 2051–2100, indicating that flood risk is likely to increase in the future in the HJR Basin due to the climate change alone without further changes in hydrological engineering and flood management. The results quantified the flood frequency under nonstationarity conditions with physically based covariates and provided information to the decision-makers to address the potential risks posed to the HJR Basin.

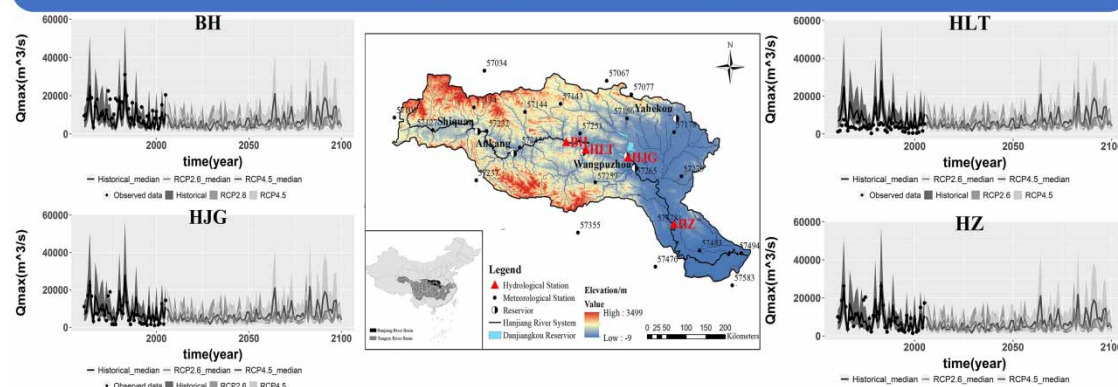
Key words: climate change, flood frequency, GAMLSS, Hanjiang River Basin, nonstationarity

HIGHLIGHTS

- The nonstationary model with physically based explanatory covariates can better describe the flood regime.
- The model analyzes the changes in the annual maximum streamflow over time and association with climatic and reservoir indices.
- Flood risk is likely to increase in the future in the Hanjiang River Basin due to climate change alone without further changes in hydrological engineering and flood management.

GRAPHICAL ABSTRACT

Evaluation and projection of annual maximum streamflow in response to anthropogenic and climatic effects under nonstationary conditions in the Hanjiang River Basin, China



CONCLUSION: The detailed information of the change of annual maximum streamflow series can be better described by physically-based nonstationary model using climatic and anthropogenic factors. The risk of flood is likely to increase over the HJR Basin without the consideration of changes in hydrological engineering and flood management in the future.

1. INTRODUCTION

Extreme hydrological and climatic events are expected to become more frequent and severe in many regions due to the considerable impacts of global climate change and human activities over the past decades (Ye *et al.* 2013). The warming climate tends to intensify the hydrological cycle at global and continental scales (Apurv *et al.* 2015), which has the potential to change the spatio-temporal characteristics of extreme hydrological and climatic events. The changes in extreme hydrological and climatic events such as more extreme precipitation, higher water levels and streamflow, potentially triggering more floods, have been widely reported (Zhai *et al.* 2005; Min *et al.* 2011; Donat *et al.* 2016; Wu & Polvani 2017). Mallakpour & Villarini (2015) detected an increasing frequency of floods over the central United States and pointed out that the increases were caused by climate change. The same results were also found in the Pearl River of China (Chen *et al.* 2009), central Germany (Petrov & Merz 2009) and the west and north UK (Hannaford & Marsh 2008). Besides, intensifying human activities such as urbanization, agriculture and construction of water reservoirs has a significant impact on the underlying surface, leading to changes in flood regimes and making the flood no longer follow a simple, natural process. Zhou *et al.* (2013) found that urbanization has a remarkable impact on surface runoff and base flow. Zhang *et al.* (2015b) found that the construction of water reservoirs was the important factor influencing the flood frequency. All these factors including climate change and human activities alter the hydrological processes and trigger nonstationarity in hydrologic time series, and make the use of traditional hydrological frequency analysis methods based on the assumption of stationarity invalid.

Thus, nonstationary analysis of hydrologic time series has been attracting increasing attention and numerous studies have been reported that attempt to address frequency analysis with the consideration of nonstationarity (Galloway 2011; López & Francés 2013; Panagoulia *et al.* 2014; Hao *et al.* 2019b). The most common way to analyze nonstationarity of hydrologic time series is to associate the distribution parameters with time by linear relationship in a changing environment (Villarini *et al.* 2010; Xu & Huang 2011; Zhang *et al.* 2014; Mullan *et al.* 2016), but unfortunately this cannot help to reveal the physical mechanisms behind the changing properties. The irrationality of this method is that the different trends such as rising, falling and jumping, identified based on the historical observations, cannot be revealed in the future, making their usefulness in understanding the risks of future extreme events limited. To date, many studies have reported that the distribution parameters of candidate probability distribution, in terms of extreme precipitation, flood event, extreme water level and drought event, are dependent on time (Cunderlik & Ouarda 2006) or some physical covariates (e.g., climate indices, urbanization and

water reservoir construction; see, for example, Zhang *et al.* 2015b; Liu *et al.* 2017; Hao *et al.* 2019b). Moreover, Hao *et al.* (2019b) and Zhang *et al.* (2015b) pointed out that adopting the physical factors as covariates in modeling the hydrologic events can better describe the changing properties of hydrological events and aid better understanding of the physical mechanisms behind the changing properties. For this reason, Villarini *et al.* (2009a) developed a framework for flood frequency analysis with nonstationarity based on the Generalized Additive Models for Location, Scale and Shape (GAMLSS) parameters, a tool for allowing all the distribution parameters to be modeled as linear/nonlinear or smooth functions of explanatory variables. GAMLSS has been widely used in nonstationary analysis with explanatory variables in hydrology and can obtain better simulation results (Zhang *et al.* 2015a; Gu *et al.* 2016; Wu *et al.* 2021). To present the nonstationary characteristics of flood processes, the parameters of the candidate distribution have often been assumed to be varied as a function of explanatory variables (Villarini *et al.* 2009a, 2009b; Zhang *et al.* 2015a). Clear evidence shows that climate change and human activities can lead to changes in the flood process. Climate change can lead to atmospheric circulation anomalies, which has a profound impact on the distribution of global large-scale water vapor and precipitation regimes. Changes in large-scale precipitation regimes have a certain impact on regional extreme precipitation, thereby affecting the regional flood processes (Fang *et al.* 2014). On the other hand, global warming boosts the atmosphere's water-holding capacity, thus directly affecting precipitation and then flood processes (Trenberth 2011). Thus, precipitation and temperature are the most important climatic variables influencing the flood processes. Human activity, especially the construction of water reservoirs, also impacts rainfall-runoff processes and is another important explanatory factor. However, due to the difficulty of quantifying the impact of human activities on the flood processes, research on the understanding of flood processes under the effect of human activities, particularly the joint effect of human activities and climate change, is limited. Studies to address this issue will benefit the understanding of the regional hydrological responses of floods to climate change and human activities and provide significant information for developing strategies of mitigation and adaptation to climate change and human activities' impacts on flood in flood-prone areas such as our study area, the HJR Basin.

The HJR Basin is an extremely sensitive area to climate change (Chen *et al.* 2015). Flood disasters occur frequently in this basin. Historically, the HJR Basin has suffered numerous devastating floods causing great damages in economy and infrastructure in 1981, 1983, 2003, 2005, 2007, 2010 and 2011 (Jin 1986; Qin 1991; Wang *et al.* 2007; Yin & Huang 2012; Xiao *et al.* 2013), making it the most serious flood disaster area in each sub-basin of the Yangtze River Basin. For example, rare floods caused by continuous rainstorm resulted in a disaster in the Hanzhong area of the HJR Basin in 1981. Then in 1983, the continuous regional heavy precipitation led to a catastrophic flood, which brought a devastating disaster to the Ankang City in the HJR Basin. In addition, the key flood control project, the Danjiangkou Reservoir (DJKR), is located in the middle and upper reaches of the HJR. The DJKR is the water source of the Middle Route of the South-to-North Water Diversion Project and plays an important role in promoting the sustainable development of national economy and the improvement of the ecological environment in northern China (Hao *et al.* 2019b). However, due to climate change and human activities, the characteristics of flood process in the HJR Basin have changed, which leads to the previous research results under the stationarity condition no longer being applicable to the changing environment. Therefore, it is of great significance to carry out the study of nonstationary flood events in the HJR Basin under a changing environment.

The objectives of this study are: (1) to develop a nonstationary model of the annual maximum streamflow (AMS) based on the GAMLSS in the HJR Basin; (2) to investigate the changing characteristics of the AMS over time and association with climatic and reservoir indices and (3) to predict the changing features of the AMS in the future with an optimal predictive model with climatic and reservoir indices. This study is expected to benefit the understanding of the changing properties of flood regimes and provide significant information for the estimation of flood events in the changing environment, and is important for policymakers and practitioners to design, maintain and manage water resource infrastructures to protect people's life and property and ensure safety in the HJR Basin.

2. STUDY REGION AND DATA

2.1. Study region

The HJR (see Figure 1) is the longest tributary of the Yangtze River with a length of 1,557 km. Originating from the southern slope of Qinling Mountains at an elevation of about 3,500 m a.s.l., the HJR flows eastward through the Jiangnan Plain at an elevation of about 30 m a.s.l. before discharging into the Yangtze River at the Wuhan City of the Hubei Province (Zhu *et al.* 2008). Located between 30°08'–34°11'N and 106°12'–114°14'E, extending about 900 km from west to east and about 460 km

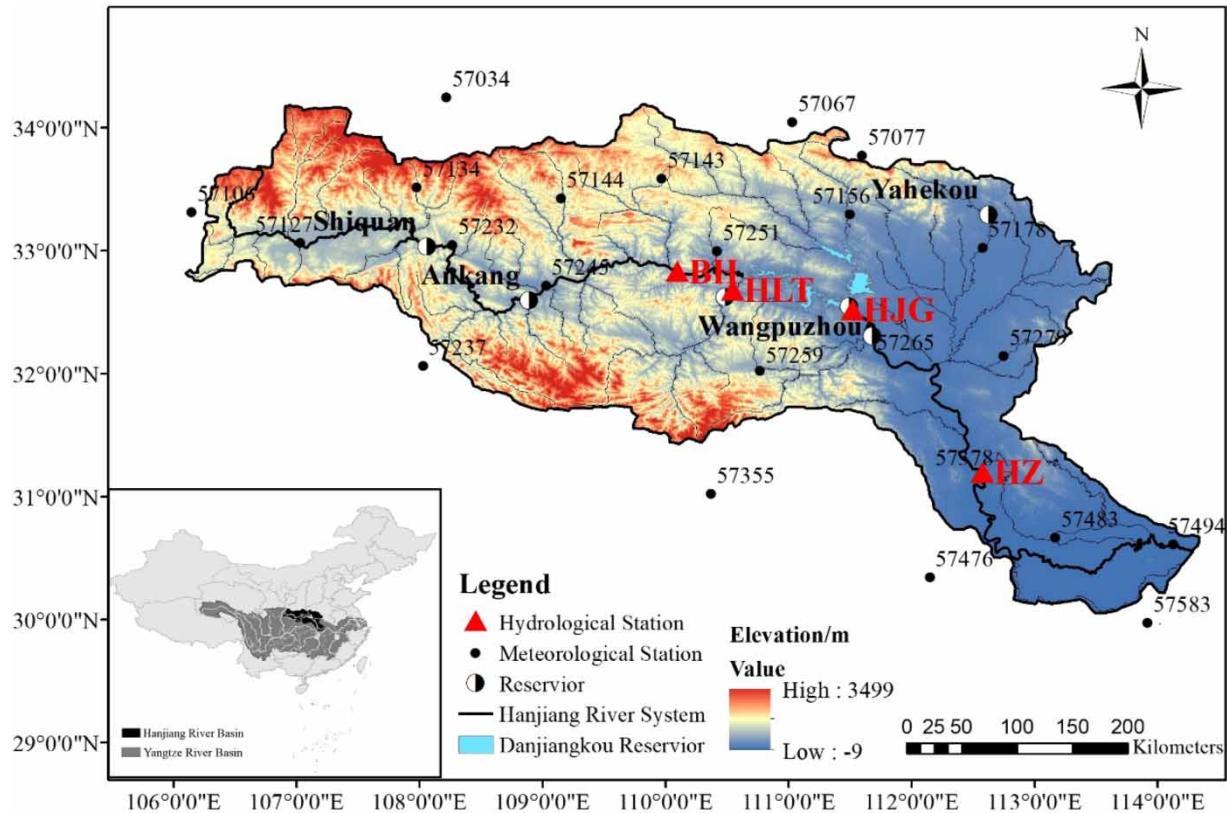


Figure 1 | Summary of the HJR Basin with the locations of hydrological stations, meteorological stations and water reservoirs.

from south to north, the HJR Basin is situated in the central part of China with a total area of 159,000 km² and exhibits a variety of geological and climatic features (Hao *et al.* 2019a). The climate of the HJR Basin is mainly controlled by sub-tropical monsoon, with the average annual air temperature ranging from 15 to 17 °C and precipitation varying from 700 to 1,800 mm, respectively. Precipitation during June–October accounts for 70–80% of the annual total, with big inter-annual variations and an uneven distribution in the HJR Basin (Shi *et al.* 2002; Yang *et al.* 2015). The runoff during June–October accounts for about 75% of the annual total and is closely related to rainfall in the HJR Basin (Hao *et al.* 2019b). Extreme precipitation and flood disasters occur frequently in this region.

The DJKR, consisting of Dan Reservoir and Han Reservoir, was constructed over the period of 1958–1973 (Hao *et al.* 2019b). Located in the upper reaches of the HJR, the DJKR is the important water source of the Middle Route of the South-to-North Water Diversion Project and utilized to satisfy the water demand of major cities, such as Beijing and Tianjin. Besides, the DJKR is the key hydraulic project in the HJR Basin, with the comprehensive functions of flood control, irrigation, power generation and navigation. The HJR is one of the important freshwater aquacultures in China and is of crucial importance for both economy and ecology in this region. Being affected by climate change and intense human activities in recent years, the hydrological processes tend to change as reflected by more extreme hydrological events in the HJR Basin during the last decades (Chen *et al.* 2015; Tao *et al.* 2015; Yang *et al.* 2015). Therefore, analyzing the nonstationarity of the flood under the changing environment is of great importance to understand the changing flood regimes and its physical mechanisms, which is critical to flood control and disaster reduction in the HJR Basin.

2.2. Data

2.2.1. Local data set

Meteorological data from 1961 to 2005 for 23 meteorological stations, which were obtained from China Meteorology Administration (CMA) and the National Climate Center, including daily observations of air temperatures and precipitation, were used in this study. The locations of meteorological stations over the HJR Basin are shown in Figure 1, from which it can

be seen that the stations are well distributed in space and therefore can reflect the characteristics of regional climate. Among these stations, 15 are within the HJR Basin and the rest are outside but close to the edges of the basin. The detailed information for these meteorological stations is shown in Table 1. The missing data for 1–2 days were filled by the average value of the neighboring days. Data missing for consecutive days were filled by using the average values of the same days of other years. In this study, the regional average precipitation and temperature of the HJR Basin were calculated based on the daily observations from the 23 stations by using the Thiessen polygon method (Thiessen 1911).

Daily streamflow data for the period 1961–2005, which were provided by the Hydrology Bureau of Changjiang Water Resources Commission, were collected from four hydrological stations, i.e., Baihe (BH), Huangjiagang (HJG), Huanglongtan (HLT) and Huangzhuang (HZ), in the HJR Basin. The quality of data was firmly controlled before its release, and there were no missing values in these flow data. As the maximum streamflow value estimates are important for flood risk assessment and also for the design of hydraulic structures, the AMS series were used to analyze the nonstationarity in flood frequency in this paper.

The locations of the four stations over the HJR Basin can be referred in Figure 1 and detailed information of these hydrological stations is given in Table 2. BH and HJG stations, located on the middle stream of the HJR, are the control hydrological stations of inflow and outflow for the DJKR, respectively. The HLT station is located on the Du river, a tributary of the HJR. The HZ station is located in the downstream of the HJR, 241 km below the DJKR. Figure 1 shows six major reservoirs, i.e., Shiquan, Danjiangkou, Ankang, HLT, Yahekou and Wangpuzhou, with a total storage capacity of $2.33 \times 10^{11} \text{ m}^3$. Detailed information of these six reservoirs in the HJR Basin is shown in Table 3.

2.2.2. Large-scale data set

Twenty-six large-scale atmospheric reanalysis data for the period 1961–2005, collected from the National Centers for Environmental Prediction (NCEP) and National Center for Atmospheric Research (NCAR) project, were used as

Table 1 | Information of 23 meteorological stations considered in the HJR Basin in this study

Station ID	Station name	Lat_N	Long_E	Alt_m
57034	Wugong	108.22	34.25	447.80
57067	Lushi	111.03	34.05	568.80
57077	Luanchuan	111.60	33.78	750.30
57106	Lveyang	106.15	33.32	794.20
57127	Hanzhong	107.03	33.07	509.50
57134	Foping	107.98	33.52	827.20
57143	Shangzhou	109.97	33.59	742.20
57144	Zhenan	109.15	33.43	693.70
57156	Xixia	111.50	33.30	250.30
57178	Nanyang	112.58	33.03	129.20
57232	Shiquan	108.27	33.05	484.90
57237	Wanyuan	108.03	32.07	674.00
57245	Ankang	109.03	32.72	290.80
57251	Yunxi	110.42	33.00	249.10
57259	Fangxian	110.77	32.03	426.90
57265	Laohekou	111.67	32.38	90.00
57279	Zaoyang	112.75	32.15	125.90
57355	Badong	110.37	31.03	334.00
57378	Zhongxiang	112.57	31.17	65.80
57476	Jingzhou	112.15	30.35	32.20
57483	Tianmen	113.17	30.67	34.10
57494	Wuhan	114.13	30.62	23.10
57583	Jiayu	113.92	29.98	36.00

Table 2 | Information of the four hydrological stations considered in the HJR Basin in this study

Stations	Long_E	Lat_N	Drainage area (km ²)	Annual average streamflow (10 ⁹ m ³)
Baihe	110.1	32.83	59,115	209.97
Huangjiagang	111.52	32.52	95,217	355.81
Huanglongtan	110.55	32.68	10,668	54.92
Huangzhuang	112.58	31.2	142,056	465.97

Table 3 | Information of the six reservoirs considered in the HJR Basin in this study

Reservoir name	Long_E	Lat_N	Drainage area (km ²)	Total storage capacity (10 ⁹ m ³)	Construction period
Shiquan	108.057	33.035	24,000	4.4	1971–1975
Danjiangkou	111.49	32.55	95,200	174.5	1958–1973
Ankang	108.89	32.6	35,700	25.85	1982–1992
Huanglongtan	110.48	32.627	11,140	11.625	1969–1978
Yahekou	112.625	33.296	3,030	13.39	1958–1960
Wangpuzhou	111.68	32.31	95,886	3.095	1993–2001

atmospheric predictor variables representing the present condition to calibrate and validate the Statistical Downscaling Model (SDSM, Wilby *et al.* 2002; Velautham *et al.* 2017). Luo *et al.* (2020) pointed out that the updated CMIP6 models show no significant difference from their counterpart CMIP5 for some models by comparing different versions of models from the same organization. In addition, the output from CanESM2 in CMIP5 can better model the atmospheric data in China, and the data of CanESM2 were processed by the Canadian Centre for Climate Modelling and Analysis (CCCma), which can be directly used for the SDSM (Dagnenet & Markus 2018; Liu *et al.* 2019). Therefore, the CanESM2 in CMIP5 was employed to predict the future climate in the HJR Basin in this study. The second generation of the Earth System Model CanESM2, developed by the CCCma of Environment and Climate Change Canada, is the fourth generation of the coupled global climate model (GCM) used for the construction of daily local meteorological variables for future climate projection based on the validated SDSM (Li & Barker 2005; von Salzen *et al.* 2005). The CanESM2 outputs are available for the whole global model with a uniform longitude resolution of 2.8125° and nearly uniform latitude resolution of roughly 2.8125° (Dagnenet & Markus 2018). The resolution of NCEP/NCAR reanalysis data was interpolated to the CanESM2 resolution of 2.8125°×2.8125°. The 26 large-scale atmospheric predictor variables of the NCEP/NCAR for the period 1961–2005 and CanESM2 outputs for the period 2006–2100, downloaded from the Internet (<http://climate-scenarios.canada.ca/?page=pred-canesm2>), are shown in Table 4. The CanESM2 outputs include three different climate scenarios: a very low forcing level (RCP2.6), a medium stabilization scenario (RCP4.5) and a very high baseline emission scenario (RCP8.5). The RCP2.6 scenario aims to limit the increase of global mean temperature unlikely to exceed 2 °C, whereas the RCP4.5 scenario aims to limit the increase of global mean temperature closer to 2 °C (Wang *et al.* 2019). In the light of the 2015 Paris Agreement, which aims to limit global warming well below 2 °C, the RCP2.6 and RCP4.5 scenarios were selected in this study to investigate the possible effect on flooding until the end of the 21st century.

3. METHODOLOGY

3.1. Description of the SDSM

The SDSM, described as a combination of stochastic weather generator and multiple regression-based statistical methods developed by Wilby *et al.* (2002), is a decision support tool for generating future weather variables to assess the impact of local climate change. The SDSM is widely used in the assessment of regional hydrological response to climate change through the relationships between local predictands of interest (e.g., precipitation and temperature) and large-scale predictors (NCEP and GCM) of the study area constructed by the validated SDSM (Wang *et al.* 2013; Dagnenet & Markus 2018; Wang *et al.* 2019). In this study, the SDSM was applied in the HJR Basin to downscale the regional daily temperature and

Table 4 | Information of 26 large-scale atmospheric predictor variables used in this study

Predictor name	Description	Predictor name	Description
mslpgl	Mean sea level pressure	p5zhgl	500 hPa Divergence of true wind
p1_fgl	1,000 hPa Wind speed	p850gl	850 hPa Geopotential
p1_ugl	1,000 hPa Zonal wind component	p8_fgl	850 hPa Wind speed
p1_vgl	1,000 hPa Meridional wind component	p8_ugl	850 hPa Zonal wind component
p1_zgl	1,000 hPa Relative vorticity of true wind	p8_vgl	850 hPa Meridional wind component
p1thgl	1,000 hPa Wind direction	p8_zgl	850 hPa Relative vorticity of true wind
p1zhgl	1,000 hPa Divergence of true wind	p8thgl	850 hPa Wind direction
p500gl	500 hPa Geopotential	p8zhgl	850 hPa Divergence of true wind
p5_fgl	500 hPa Wind speed	prcpgl	Total precipitation
p5_ugl	500 hPa Zonal wind component	s500gl	500 hPa specific humidity
p5_vgl	500 hPa Meridional wind component	s850gl	850 hPa Specific humidity
p5_zgl	500 hPa Relative vorticity of true wind	shumgl	1,000 hPa Specific humidity
p5thgl	500 hPa Wind direction	tempgl	Air temperature at 2 m

precipitation with a number of steps such as quality control and data transformation, screen variables, model calibration, weather and scenario generator. For more detailed steps and procedures, readers can refer to [Wilby *et al.* \(2002\)](#) for further reading. The selection of appropriate predictors is a critical step in the development of the SDSM and can significantly affect its realization and stability. In the predictor selection processes, all 26 atmospheric variables were treated as potential predictors and the appropriate predictors were selected using the stepwise multi-linear regression method with a confidence level of 0.001. Besides, correlation analysis and partial correlation analysis were also considered in the predictor selection between selected predictors and predictand.

With the consideration of seasonality, the relationships between selected predictors and predictand variables in the HJR Basin are established through calibration and validation for each month of the year where 12 regression equations are derived for 12 months using different regression parameters for each month's equation. The observations and NCEP reanalysis data of the period 1961–2005, representing the current climate, were divided into two sub-period data sets. The data for the period 1961–1990 were used for model calibration, and the remaining 15-year data for the period 1991–2005 were used for model validation.

To assess the performance of the regression SDSM, three statistical indicators, i.e., the coefficient of determination (R^2), the coefficient of efficiency (Nash–Sutcliffe efficiency, NSE) and the ratio of simulated and observed standard deviation (RS), were employed in this study ([Hundechea & Bardossy 2008](#); [Wang *et al.* 2013](#)) and are given below.

$$NSE = 1 - \frac{\sum_{i=1}^N (O_i - S_i)^2}{\sum_{i=1}^N (O_i - \bar{O})^2} \quad (1)$$

$$RS = \frac{S_{sim}}{S_{obs}} \quad (2)$$

where N is the number of samples; O_i is the value of observation; S_i is the value of the simulated predictand; S_{sim} is the standard deviation of the modeled series calculated by the SDSM and S_{obs} is the standard deviation of the observed series. The closer the values of R^2 , NSE and RS to 1, the more successfully the SDSM model performed. In this study, the future precipitation and temperature were projected using the SDSM to analyze future changes in climate.

3.2. Generalized Additive Models for Location, Scale and Shape

The GAMLSS, proposed by [Rigby & Stasinopoulos \(2005\)](#), was employed in this study to model the AMS series under non-stationary conditions through the development of regressive relations between distributional parameters and explanatory variables in the HJR Basin. Compared with classical generalized additive models (GAMs), GAMLSS provides a flexible choice in specifying the distribution of the response variable and also allows all the distribution parameters to be modeled as linear/nonlinear or smooth functions of explanatory variables ([Hao et al. 2019b](#)).

It is assumed that the independent observation data $y^T = (y_1, y_2, \dots, y_n)$ follows the distribution function of $F_y(Y_i/\theta_i)$ with $\theta_i = (\theta_{i1}, \theta_{i2}, \dots, \theta_{ip})$ denoting the distributional parameters and p denoting the number of parameters. The distributional parameters are related to the explanatory variables by the monotonic link function $g_k(\cdot)$ with $k = 1, 2, \dots, p$. The monotonic link function developing a relationship between distributional parameters and explanatory variables can be computed by:

$$g_k(\theta_k) = X_k \beta_k + \sum_{j=1}^m h_{jk}(x_{jk}) \quad (3)$$

where θ_k and β_k denote parameter vectors of length n and m , respectively; X_k is an $n \times m$ matrix of explanatory variables and h_{jk} denotes the functional dependence of the distribution parameters on explanatory variables x_{jk} . In this study, the functional dependence for the response variable was constructed based on Penalized splines (P-splines) smoother. P-splines, introduced by [Eilers & Marx \(1996\)](#), are piecewise polynomials defined by B-spline basis functions in the explanatory variable, where the coefficients of the basis functions are penalized to guarantee sufficient smoothness. Five widely used distributions with two parameters (θ_1 and θ_2), including Gumbel distribution (GU), Weibull distribution (WEI), Gamma distribution (GA), Lognormal distribution (LOGNO) and Logistic distribution (LO), were used for the candidate distribution function in modeling flood data ([Rigby & Stasinopoulos 2005](#)). The θ_1 and θ_2 are characterized as location and scale parameters, respectively. Detailed information about the five distributions is shown in [Table 5](#). Three models were considered in this paper for analyzing the AMS series:

Table 5 | Summary of the five distributions considered in this study

PDF		Link functions	
		θ_1	θ_2
Weibull	$f_Y(y \theta_1, \theta_2) = \frac{\theta_2 y^{\theta_2-1}}{\theta_1^{\theta_2}} \exp\left\{-\left(\frac{y}{\theta_1}\right)^{\theta_2}\right\}$ $y > 0, \theta_1 > 0, \theta_2 > 0$	Log	Log
Gamma	$f_Y(y \theta_1, \theta_2) = \frac{1}{(\theta_2^2 \theta_1)^{1/\theta_2}} \frac{y^{(1/\theta_2)-1} \exp(-y/\theta_2^2 \theta_1)}{\Gamma(1/\theta_2)}$ $y > 0, \theta_1 > 0, \theta_2 > 0$	Log	Log
Lognormal	$f_Y(y \theta_1, \theta_2) = \frac{1}{\sqrt{2\pi\theta_2^2}} \frac{1}{y} \exp\left\{-\frac{[\log(y) - \theta_1]^2}{2\theta_2^2}\right\}$ $y > 0, \theta_1 > 0, \theta_2 > 0$	Identity	Log
Logistic	$f_Y(y \theta_1, \theta_2) = \frac{\exp\left(\frac{y - \theta_1}{\theta_2}\right)}{\theta_2 \left[1 + \exp\left(\frac{y - \theta_1}{\theta_2}\right)\right]^2}$ $-\infty < y < \infty, -\infty < \theta_1, \theta_2 > 0$	Identity	Log
Gumbel	$f_Y(y \theta_1, \theta_2) = \frac{1}{\theta_2} \exp\left\{-\left(\frac{y - \theta_1}{\theta_2}\right) - \exp\left[-\left(\frac{y - \theta_1}{\theta_2}\right)\right]\right\}$ $-\infty < y < \infty, -\infty < \theta_1 < \infty, \theta_2 > 0$	Identity	Log

- Stationary model 0: the parameters of distribution are constant.
- Nonstationary model 1: the parameters of distribution change with time.
- Nonstationary model 2: the parameters of distribution change with climatic covariate (precipitation or temperature) and anthropogenic covariate (reservoir index (RI)).

The Akaike's information criterion (AIC; Akaike 1974) was employed to select the most efficient model. Backward step-wise model selection through a series of tests (e.g., *F*-tests, *t*-tests) was used to find a set of independent variables that significantly influence the dependent variable. To evaluate the goodness of fit of the optimal models, the independence and normality of the (normalized quantile) residuals were checked by computing the Filliben coefficient (Filliben 1975), together with the worm plots (Buuren & Fredriks 2001). In this study, the nonstationary characteristics of AMS were investigated based on the optimal nonstationary model 2, as well as the investigation of the future flood frequency with future anthropogenic and climatic factors.

3.3. Reservoir index

The RI, proposed by López & Francés (2013), was employed in this study to describe the impact of regulations of dams or reservoirs on flood regimes. The method of calculating the RI is given as:

$$RI = \sum_{i=1}^N \left(\frac{A_i}{A_T} \right) \left(\frac{C_i}{C_T} \right) \quad (4)$$

where N is the number of reservoirs or dams upstream of the hydrological station; A_T denotes the drainage area of the hydrological station; A_i denotes the drainage area of each reservoir; C_T denotes the mean annual runoff at the hydrological station and C_i denotes the total capacity of each reservoir.

4. RESULTS AND DISCUSSION

4.1. RI changes

Six major reservoirs, i.e., Shiquan, Danjiangkou, Ankang, HLT, Yahekou and Wangpuzhou, which significantly affect the flood regimes in the HJR Basin, were analyzed in this study to present the influence of the anthropogenic factor on flood processes. The locations of the six reservoirs over the HJR Basin are shown in Figure 1. Figure 2 shows the changes in the AMS and RI at the four hydrological stations. It can be seen from Figure 2 that the AMS series fluctuates at a low level when the value of RI is relatively high. Figure 1 shows that the HJG station is close to the DJKR, which was completed in 1975. Figure 2 also shows high alterations of flood regime at the HJG station influenced by the DJKR with the value of $RI = 0.49$ after 1975, which is in line with the completion time of the DJKR. Zhang *et al.* (2015b) pointed out that the threshold value of $RI = 0.25$ is between low reservoir- and high reservoir-induced alterations. In the upstream of the BH station, there are two reservoirs such as Shiquan and Ankang reservoirs. Figure 2 shows that $RI = 0.08$, implying low impacts of the Shiquan reservoir on flood regimes at the BH station. A relatively high alteration of the flood regime can be observed after the 1990s, which is in line with the completion time of the Ankang reservoir. Figure 2 also indicates that alterations of flood regimes after 1975 (the completion time of the Shiquan reservoir) are lower than those after the 1990s, showing a relatively low impact of the Shiquan reservoir on flood regimes at the BH station. The HLT station located at the tributary of the HJR is only influenced by the HLT reservoir (Figure 1). Figure 2 indicates that $RI = 0.22$, showing a relatively low impact of the HLT reservoir on flood regime at the HLT station. Flood regimes at the HZ station are influenced by the DJKR with the alteration of flood processes after 1975 in comparison with the other reservoirs, which are far away from the HZ station, indicating that the influence of reservoirs on flood regimes diminishes with the distances between hydrological stations and reservoirs, which has been corroborated by previous studies (Zhou *et al.* 2012; Zhang *et al.* 2015b). Human activities such as the construction of water reservoirs are the important factors affecting the flood regimes. The reservoirs can regulate the AMS and have obvious effects on hydrological process (Li & Tan 2015; Zhang *et al.* 2015b). In conclusion, the RI can reflect the influence of the reservoirs on the flood regimes at the hydrological station to some extent and can be used as a covariate to analyze the nonstationarity of flood frequency to present the influence of the anthropogenic factor on flood processes.

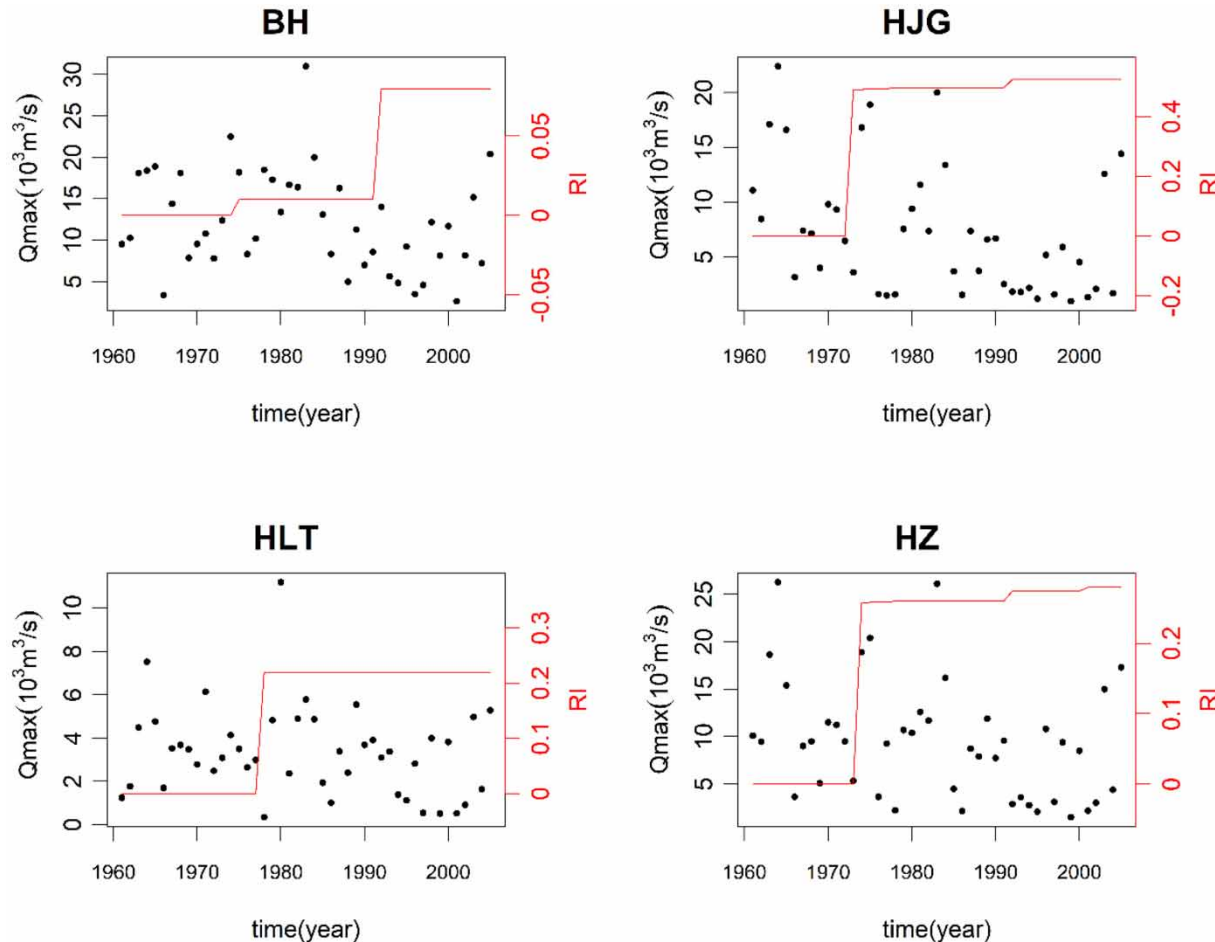


Figure 2 | Changes of the AMS series and RI at the four hydrological stations in the HJR Basin.

4.2. GAMLSS implementation

Before proceeding to nonstationary frequency analysis, the Modified Mann–Kendall test (Hamed & Rao 1998; Yue & Wang 2004) was employed to assess the significance of trend in the AMS. Results showed that decreasing trends with a significance level of 0.05 were found in the AMS at the four stations. In addition, Pearson correlation analysis between covariates (precipitation and temperature) and the AMS at the four stations was also conducted. The results indicated that the covariates and the AMS have a good correlation at the 0.05 significance level. The AMS for the four study stations in the HJR Basin were analyzed by using the GAMLSS. Table 6 summarizes the optimal distribution, Filliben correlation coefficients, AIC values and significant covariates for distribution parameters θ_1 and θ_2 for the modeling of maximum streamflow series under the three models.

It can be observed from Table 6 that the AIC values of nonstationary models 1 and 2 are smaller than those of stationary model 0, indicating that nonstationarity exists in the AMS series at the four stations. In fact, climate change and intense human activities in this area greatly alter natural hydrological processes, leading to the nonstationarity in hydrologic time series. The results of the models obtained in this study further corroborate the nonstationarity existing in the AMS. The accuracy of hydrologic analysis and design may be influenced with violation of the stationarity assumption. Many studies have shown that a constant estimated value over the study period calculated by the stationary model could not reflect the temporal changes of flood events under the influence of climate change and human activities (López & Francés 2013; Gu *et al.* 2016).

With respect to model 1, GA distribution is selected for BH, HJG and HZ stations and WEI distribution for the HLT station. Time is the significant factor influencing the parameter θ_1 (being related to the mean value of the AMS) via P-spline smoother at BH and HJG stations and linear relation at HLT and HZ stations. The parameter θ_2 (being related to the fluctuation of the AMS) at the HZ station exhibits a linear dependence on time, while the parameter θ_2 at other stations

Table 6 | Summary of the fitted distribution, Filliben correlation coefficients, AIC and significant covariates for distribution parameters θ_1 and θ_2 for the modeling of maximum streamflow series under the three models

Stations		BH	HJG	HLT	HZ
Model 0	Fitted distribution	GA	LOGNO	WEI	GA
	AIC	908.57	889.26	811.36	909.59
	Filliben	0.982	0.980	0.981	0.982
Model 1	Fitted distribution	GA	GA	WEI	GA
	θ_1	pb(t)	pb(t)	t	t
	θ_2	ct	ct	ct	t
	AIC	900.12	878.92	808.94	901.6
	Filliben	0.988	0.987	0.989	0.993
Model 2	Fitted distribution	GA	LOGNO	GA	LOGNO
	θ_1	pre + RI	pre + RI	pre + tem + RI	pb(pre) + tem + RI
	θ_2	ct	ct	ct	ct
	AIC	877.11*	846.27*	758.1*	865.54*
	Filliben	0.996	0.983	0.990	0.990

Note: Filliben coefficient >0.95 indicates high goodness-of-fit performance of the optimal models. The function pb() indicates that the dependence between parameters and external covariates is via the P-spline smoother. Variables without pb() denote linear function. ct refers to a parameter that is constant. Bold number denotes that AIC values of corresponding model are smaller than model 0. AIC values with * denote that the corresponding AIC value is the smallest.

do not change with time, i.e., being constant. Mirrored by this dependence, the temporal trends on the AMS in the HJR Basin can be detected. Figure 3 indicates the temporal variations of estimates of five quantiles (the 5th, 25th, 50th, 75th and 95th) calculated by the stationary model 0 and nonstationary model 1 for the AMS at the four stations. It can be seen from Figure 3 that the majority of the observed data points fall between the 5th and 95th quantile curves, indicating that the nonstationary

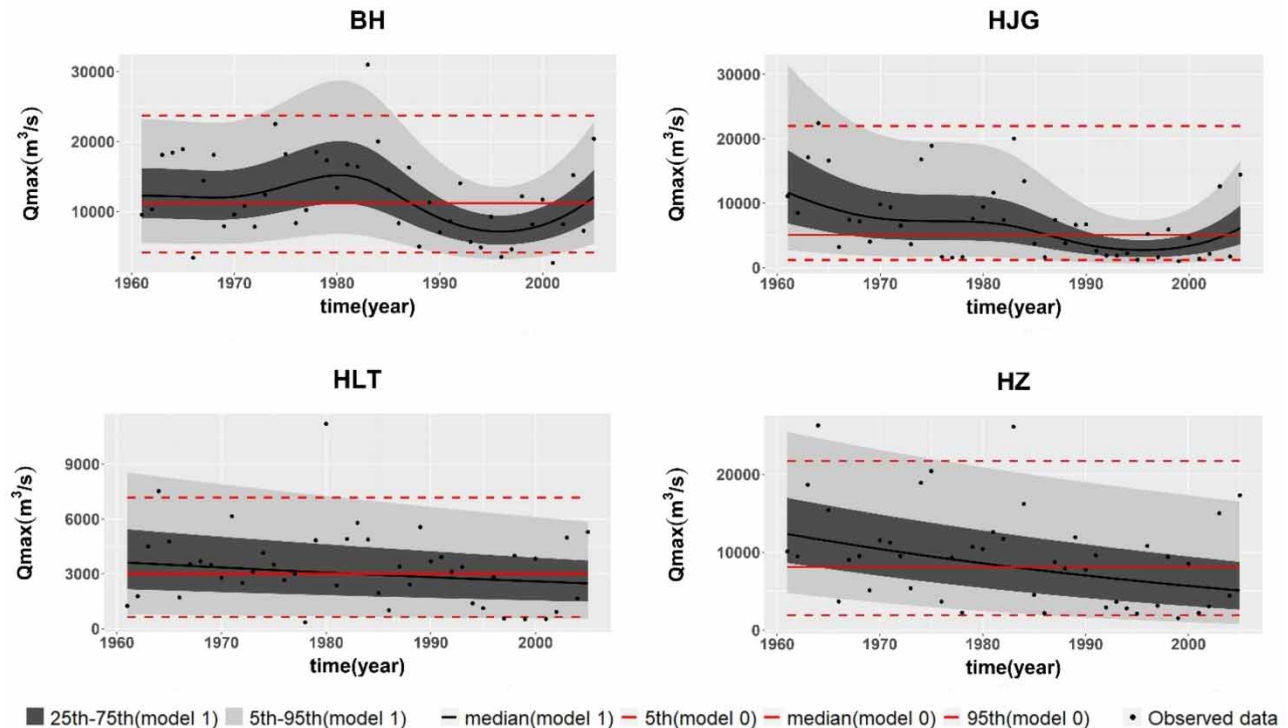


Figure 3 | Summary of the results of the stationary model 0 and nonstationary model 1 with time as the covariate for modeling the maximum streamflow series at the four stations. The solid black line denotes the 50th quantiles by model 1; the light gray region and dark gray region, respectively, denote the area between 5th and 95th quantiles and 25th and 75th quantiles by model 1; the solid red line denotes the 50th quantiles by model 0; the red dashed lines denote the 5th and 95th quantiles by model 0. Please refer to the online version of this paper to see this figure in colour: <http://dx.doi.org/10.2166/wcc.2022.376>.

model when considering the time as a covariate is able to describe the changes in the AMS. In general, as shown in Figure 3, the nonlinear (BH and HJG) or linear (HLT and HZ) decreasing trend can be observed for the AMS at the four stations. Figure 3 also indicates that the estimated quantiles of the AMS at BH and HJG stations have been increasing since 1995. The fluctuation of the AMS at the four stations decreased over the study period, especially after the completion of the reservoirs, which resulted from the regulation of the reservoirs.

It can also be observed that the AIC values of nonstationary model 2 considering the physically based covariates are the smallest among the three models, indicating that the nonstationary model 2 is selected as the optimal model. Also, the optimal variables selected in this study passed *T* test at the significance of 0.01. With respect to model 2, it can be seen from Table 6 that GA distribution has the best fitting performance for the AMS at BH and HLT stations and the optimal distribution for the AMS at HJG and HZ stations are LOGNO. Table 6 also indicates that the impacts of precipitation, temperature and RI on the AMS are identified, as reflected mainly by linear or nonlinear dependence. Precipitation, temperature and RI are the significant explanatory variables for parameter θ_1 at HLT and HZ stations. Precipitation and RI are the significant explanatory variables for parameter θ_1 at BH and HJG stations. In addition, the alterations of hydrological processes influenced by precipitation, temperature and RI have been well reported (Zhou *et al.* 2012; López & Francés 2013; Gu *et al.* 2016; Hao *et al.* 2019b). In this context, flood regimes of the HJR Basin are mainly influenced by anthropogenic and climatic effects, i.e., water reservoir, precipitation and temperature in this study.

Table 6 also summarizes the Filliben correlation coefficients for the four stations under the three models. It can be found that the Filliben coefficients are all higher than 0.98, indicating that the results of the three models can be accepted. Figures 4 and 5 are the worm plots for residuals from nonstationary models 1 and 2, respectively, from which it can be seen that all the points are inside the 95% confidence intervals, indicating a satisfactory modeling performance of the models.

4.3. Comparison of results by the three models

The AIC values for the nonstationary model 2 with precipitation, temperature and RI as covariates are the smallest. It can be observed from Figure 3 that the 5th, median and 95th quantiles by model 0 are constant and cannot describe the changing characteristics of AMS at the four stations. Model 1 can help show the trend in the 5th, 25th, 50th, 75th and 95th quantiles for the AMS and can adequately describe the changing characteristics of the AMS. However, subtle and detailed changes in the AMS cannot be fully captured by model 1 and changes of 5th and 95th quantiles in particular. Figure 6 shows the changes of estimates of five quantiles (the 5th, 25th, 50th, 75th and 95th) calculated by the nonstationary model 2 for the AMS at the four stations. As shown in Figure 6, the majority of the data points fall within the 5th–95th quantile curves, indicating that the nonstationary model 2, considering the anthropogenic and climatic factors as explanatory variables, is able to capture the subtle and detailed information of the AMS variation. The impacts of anthropogenic and climatic factors on the flood frequency at the four stations can be clearly detected. The subtle and detailed changes of different quantiles for the AMS were better described by model 2 when compared with the results of model 1 (see Figure 3), implying that the nonstationary model with its physically based explanatory covariates is more suitable to analyze the nonstationarity of hydrological extremes. As modeling AMS series with time cannot reveal the physical mechanisms behind the changing properties, the risk properties cannot be extended to the future, mainly because the changing characteristics such as rising, falling and jumping identified are based on the historical observations and include no information in the future. Historically, flood disasters occur frequently in the HJR Basin. There were different levels of floods that have occurred in this region in 1981 and 1983 (Wang *et al.* 2007; He *et al.* 2011), which can be fully captured by the nonstationary model 2 (see Figure 6). In addition, a higher fluctuation of quantiles for the AMS can be observed before 1973 than that after 1973 at HJG and HZ stations, and the time point is also the completion time of the DJKR, showing the influence of the reservoir on the flood process. Two sudden increases of estimated quantiles over the period of 1978–1985 can be observed at the four stations, indicating the influence of intensifying precipitation across the HJR Basin. However, it can be seen from Figure 3 that these flood events cannot be fully captured by model 1. Besides, Figure 7 shows the curves of estimated AMS with a return period of 20 years by models 0, 1 and 2. It can be seen from Figure 7 that the designed flood discharge calculated by model 0 is constant throughout the study period and cannot reflect the variations of the AMS under the climate change and human activities. Decreasing trends of the designed flood discharge by models 1 and 2 can be obtained according to the Modified Mann–Kendall test. Figure 7 also clearly shows the tendency. A sudden drop of estimated flood discharge can be detected in the late 1970s at the HJG and HZ stations. The time point is related to the influence of regulations by water reservoirs. Due to the precipitation extremes in 1980 and 1983, two peaks of estimated flood discharge of 20 years return period are also identified

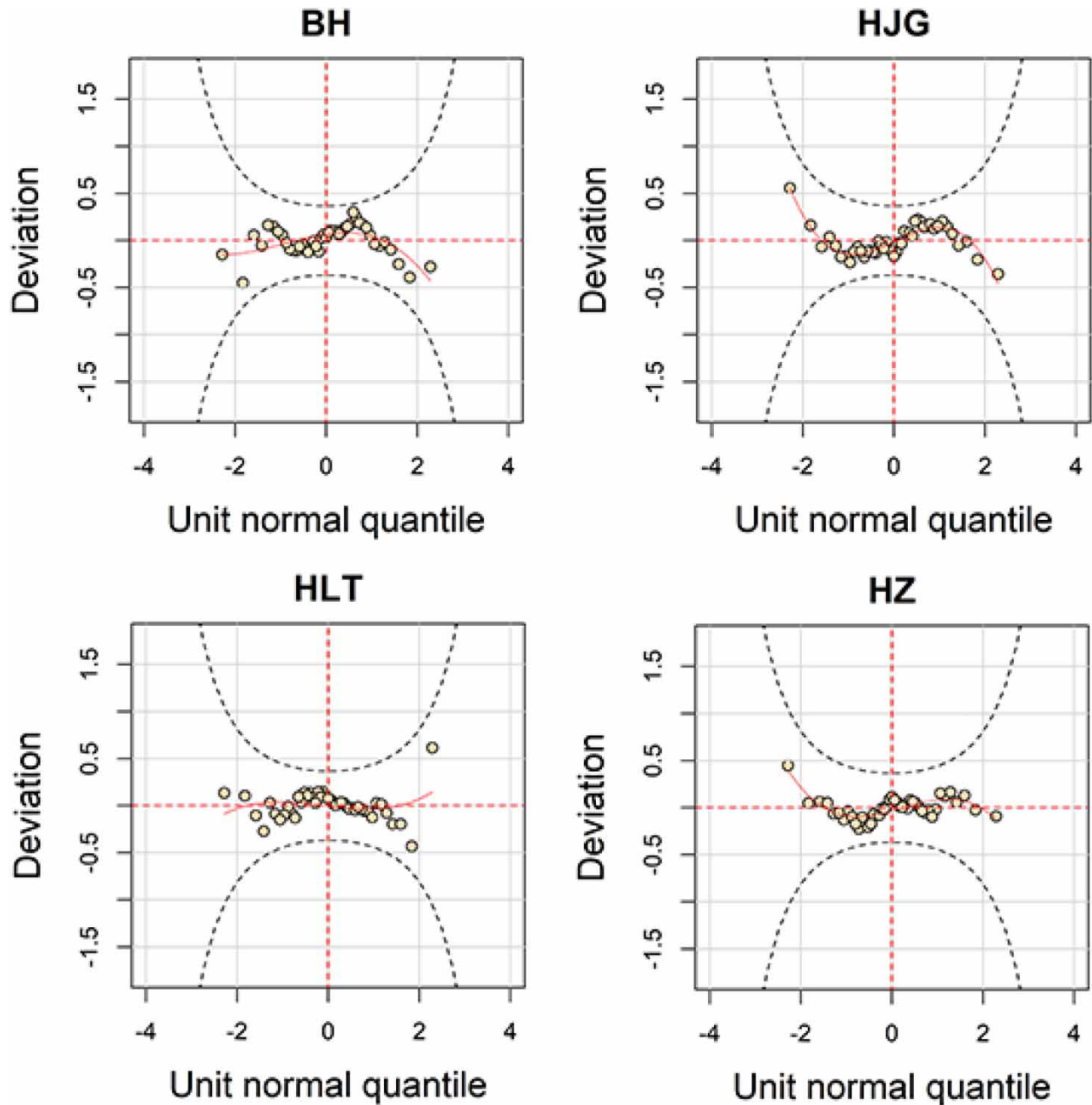


Figure 4 | Worm plots for residuals from the nonstationary model 1 for the AMS series at the four stations. The 95% confidence interval is implied by the dotted lines.

at the four stations in the HJR basin. After the 1995, the estimated flood discharge has a generally increasing tendency, showing the influence of intensifying extreme precipitation across the HJR Basin, and it is particularly the case in the upstream of the HJR Basin (Hao *et al.* 2019b). The designed flood discharge by models 0 and 1 either over- or under-estimate the real AMS and, therefore, may provide misleading results for the hydraulic design. Model 2-based estimated AMS can capture the impact of climate change and human activities on the flood process and can provide technically reasonably designed flood discharge. Figure 7 also indicates that the designed flood discharge by model 2 characterizes dramatic change on nonstationarity when compared with stationarity. In this case, the term ‘return period’ has lost its meaning and needs to be defined again (Zhang *et al.* 2015b).

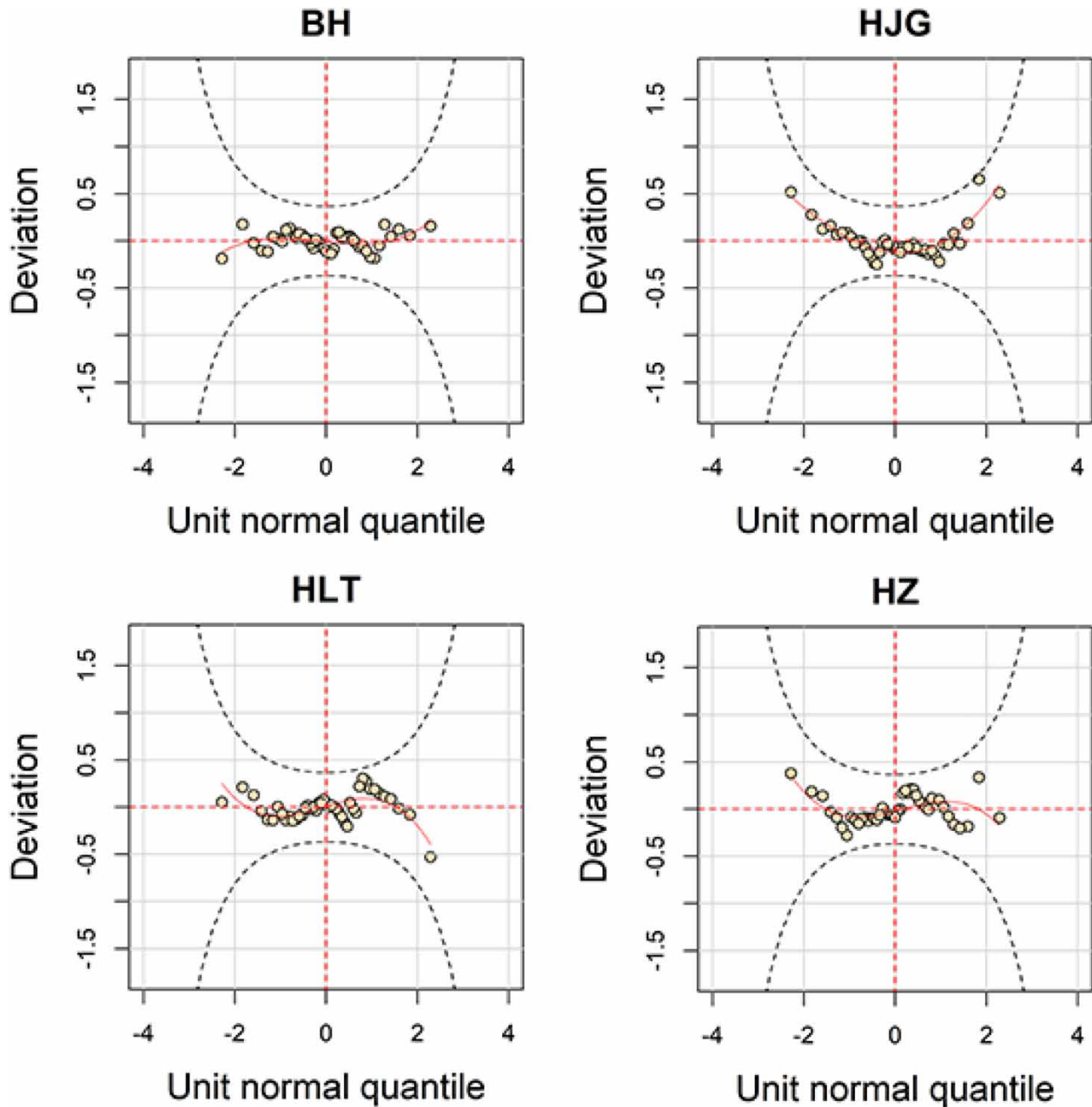


Figure 5 | Worm plots for residuals from the nonstationary model 2 for the AMS series at the four stations. The 95% confidence interval is implied by the dotted lines.

Therefore, those results indicate that climate change and human activities are the main factors influencing the flood regimes in the HJR Basin and stationarity of the AMS is largely violated. Furthermore, the increasing anthropogenic and climatic factors such as land use/land cover change and urbanization should not be ignored in the research of nonstationary flood frequency analysis (Olang & Furst 2011; Du *et al.* 2012). The main land use types in the study region were water area, cultivated land, grassland and forest land. However, with the intensification of human activities after 1980, the land use types in this area have changed. The area of water, grassland and cultivated land decreased, whereas the area of forest land and residential land increased. The land use change influenced the runoff yield and confluence, and hence influenced the AMS, which lead to the nonstationary of the AMS in the study area. Thus, incorporating more factors that have a strong influence on flood events in the nonstationary model can improve the accuracy of the results, which is helpful for improving

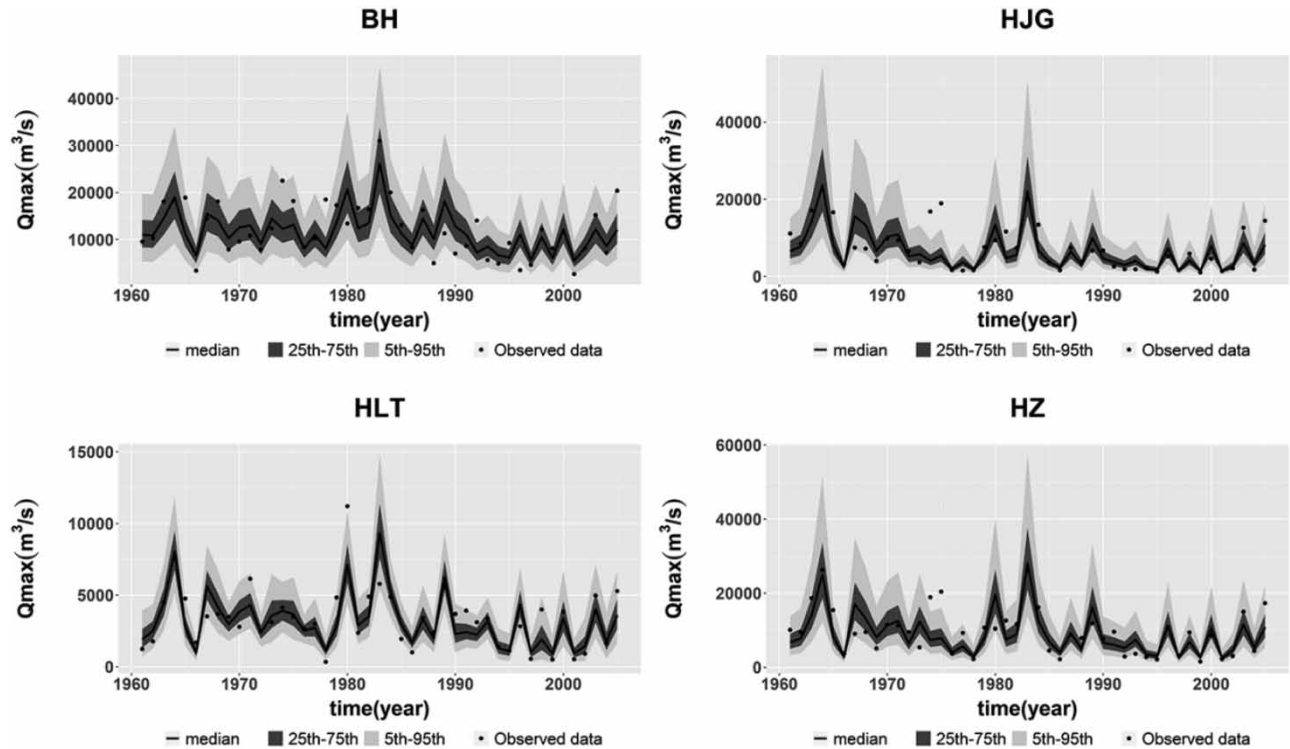


Figure 6 | Summary of the results of the nonstationary model 2 taking physically based factors as the covariates for modeling the maximum streamflow series at the four stations. The solid black line denotes the 50th quantiles; the light gray region and dark gray region, respectively, denote the area between 5th and 95th quantiles and 25th and 75th quantiles.

the simulation and prediction ability of the model. In summary, the performances of the nonstationary model 2 with physically based covariates in describing the behaviors of flood processes are better than the nonstationary model 1 in this study.

4.4. Prediction of the flood frequency under two climate scenarios

Nonstationary model 2 with anthropogenic and climatic factors as explanatory covariates, i.e., precipitation, temperature and water reservoir, can better capture the changing properties of the AMS series. In this study, the future precipitation and temperature were projected using the SDSM to analyze future changes in climate, as well as the investigation of the future AMS based on the optimal nonstationary model 2 with future anthropogenic and climatic factors.

4.4.1. Future projections of precipitation and temperature based on the SDSM

The SDSM was used to obtain the future regional daily precipitation and temperature in the HJR Basin. The results of calibration and validation are shown in Table 7, from which it can be observed that the statistical performance metrics of R^2 , Ens and RS values for temperature during the calibration and validation periods all exceed 0.97, which shows that the results for temperature perform better than that for precipitation, with the R^2 , Ens and RS values ranging from 0.43 to 0.78. The result of statistical analysis indicates that the model is much better in simulating temperature than precipitation because of the high dynamical properties of precipitation, which were mentioned in other studies (Qiu *et al.* 2010; Mekonnen & Disse 2018). Besides, the values of R^2 calculated by many researchers in the SDSM experiment for daily precipitation were between 0.2 and 0.45 (Hessami *et al.* 2007; Zhao & Xu 2007; Qiu *et al.* 2010; Mekonnen & Disse 2018), which are similar to the results obtained in this study. On the whole, this range can be accepted for practical use when dealing with precipitation downscaling because of its complexity and high spatial and temporal variabilities to downscale (Wilby *et al.* 2002; Mekonnen & Disse 2018). Therefore, the results derived from the SDSM are overall capable of representing the climate characteristics and the large-scale atmospheric reanalysis data can be used as predictors to downscale the daily precipitation and temperature by the SDSM.

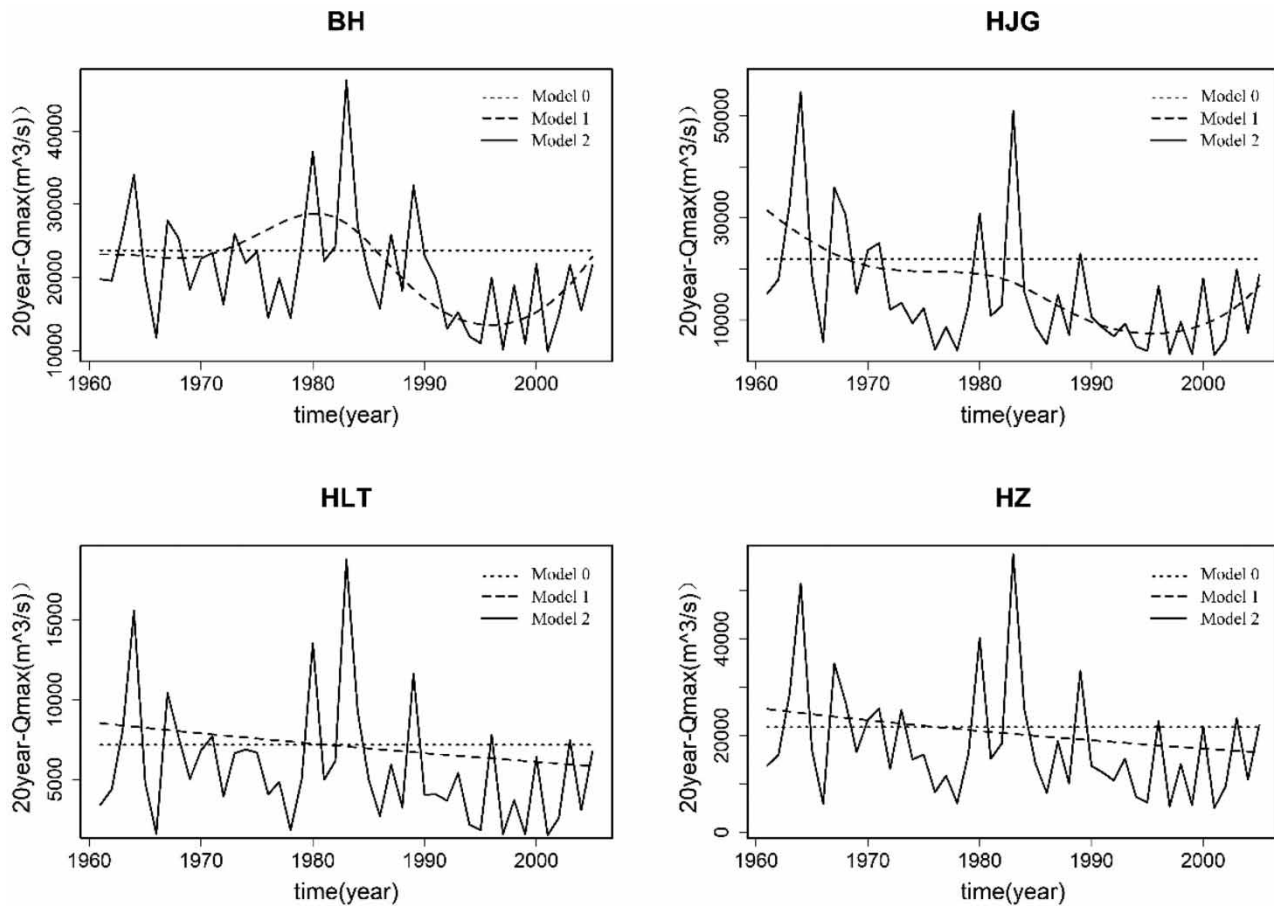


Figure 7 | Estimated flood discharge with a return period of 20 years with models 0, 1 and 2.

Table 7 | Values of three different measures between simulated and observed results of regional daily precipitation and temperature during calibration and validation periods

Period	Predictand	R^2	Ens	RS
Calibration	Precipitation	0.44	0.43	0.77
	Temperature	0.97	0.97	0.98
Validation	Precipitation	0.47	0.46	0.78
	Temperature	0.97	0.97	0.98

Table 8 shows the results of correlation coefficient R that evaluates the performance of annual data for the calibration and validation periods. Also, the curves for the calibrated and validated annual rainfall and temperature along with the observations are shown in Figure 8. The results indicated that the values of R for annual total precipitation and average

Table 8 | Performance of the annual data for calibration and validation periods

Period	Predictand	R
Calibration	Precipitation	0.75
	Temperature	0.82
Validation	Precipitation	0.70
	Temperature	0.84

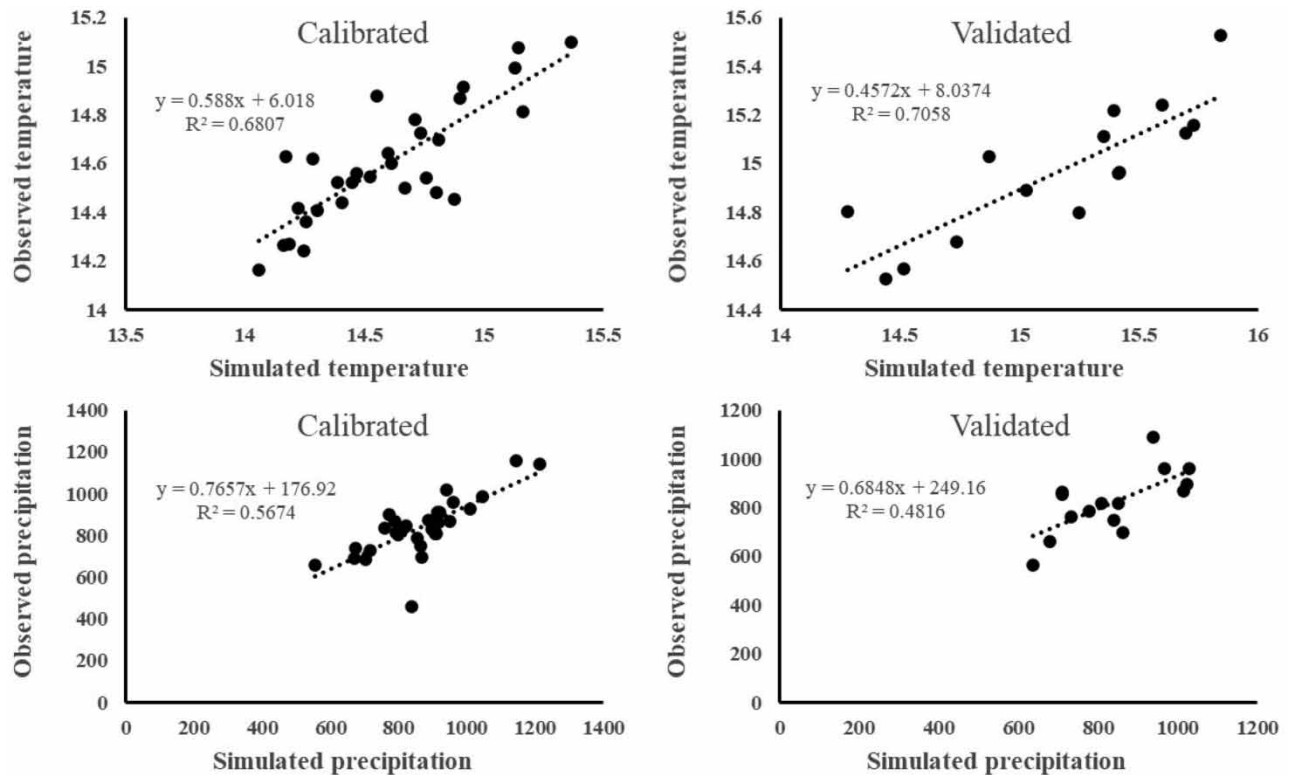


Figure 8 | Results for the calibrated and validated annual rainfall and temperature along with the observations.

temperature are larger than 0.70, indicating that the annual total precipitation and average temperature simulated by the SDSM are satisfactory and can be used as covariates in the nonstationary model. Figure 9 shows the results for the changes of total precipitation and average temperature simulated by the SDSM under the two climate scenarios (RCP2.6 and RCP4.5) over the period of 2006–2100. It can be observed that the changes of precipitation and temperature under the RCP2.6 scenario are generally consistent with that under the RCP4.5 scenario during 2006–2050. After 2050, the changes of precipitation and temperature under the RCP4.5 scenario are higher than those under the RCP2.6 scenario. In general, the total precipitation and average temperature in the HJR Basin have an upward trend over the period of 2006–2100. The result indicates an increasing trend of precipitation and temperature in the HJR Basin due to climate change, which is in line with the result from previous studies (Guo *et al.* 2009; Nie & Ding 2017). Thus, the increasing trend of precipitation and temperature in the future will influence the flood regimes in the HJR Basin, which corroborates the selection of precipitation and temperature as the covariates to reflect climate change in the nonstationarity analysis.

4.4.2. Nonstationary analysis of flood frequency under two climate scenarios

In this section, the optimal nonstationary models with the significant explanatory covariates are used for prediction of flood in terms of the 5th, median and 95th quantiles at the four stations under RCP2.6 and RCP4.5 scenarios during 2006–2100. Figure 10 shows the results for estimated quantiles projected in the future under the two climate scenarios, from which it can be observed that the changes of estimated quantiles are different under RCP2.6 and RCP4.5 scenarios. According to the Modified Mann–Kendall test, there were significant increasing trends (with the significance level of 0.05) in the AMS of the 5th, median and 95th quantiles under the RCP4.5 scenario over the period of 2006–2100, but no significant trends under the RCP2.6 scenario. During 2006–2050, the change of estimated quantiles with no significant trend under the RCP2.6 scenario is consistent with that under the RCP4.5 scenario at the four stations. During 2051–2100, the estimated quantiles are characterized by a significantly increasing trend (with the significance level of 0.05) under the RCP4.5 scenario, but no significant trend under the RCP2.6 scenario. Figure 10 indicates that the fluctuations of the AMS at the four stations are small during the period of 2006–2050, in comparison with the period of 2051–2100. In addition, because the RI of the four stations is a constant value after 2006, the changes of precipitation and temperature representing climate change are the main factors

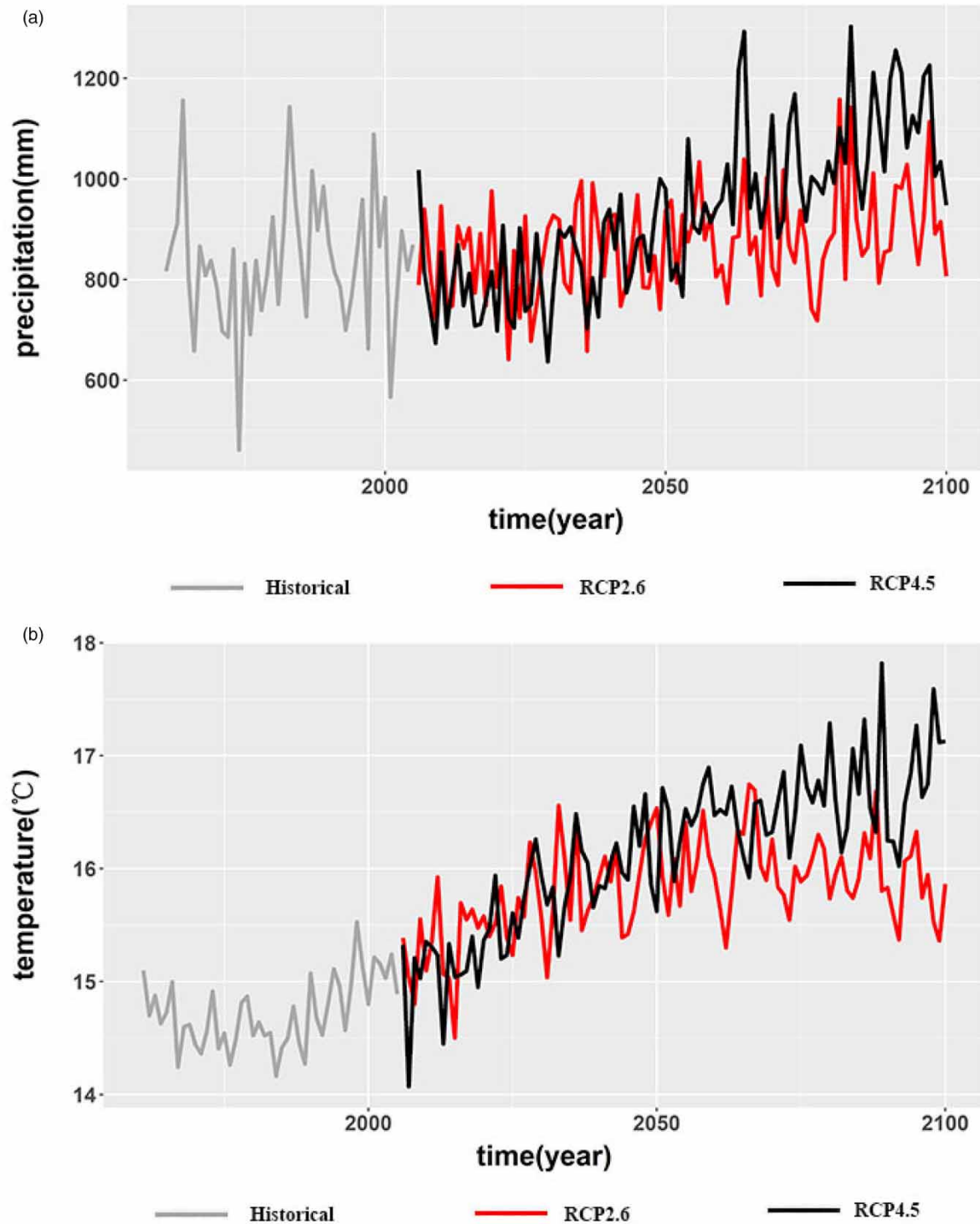


Figure 9 | Changes of (a) total precipitation and (b) average temperature simulated by the SDSM under RCP2.6 and RCP4.5 scenarios over the period of 2006–2100.

influencing the flood regimes. After 2050, the AMS at the four stations have an upward trend with the peak quantiles around 2064, 2083 and 2091, and these time points are exactly the time when heavy precipitation is found at the four stations (see [Figure 10](#)), indicating the impacts of precipitation on flood processes in the HJR Basin. These results imply that climate

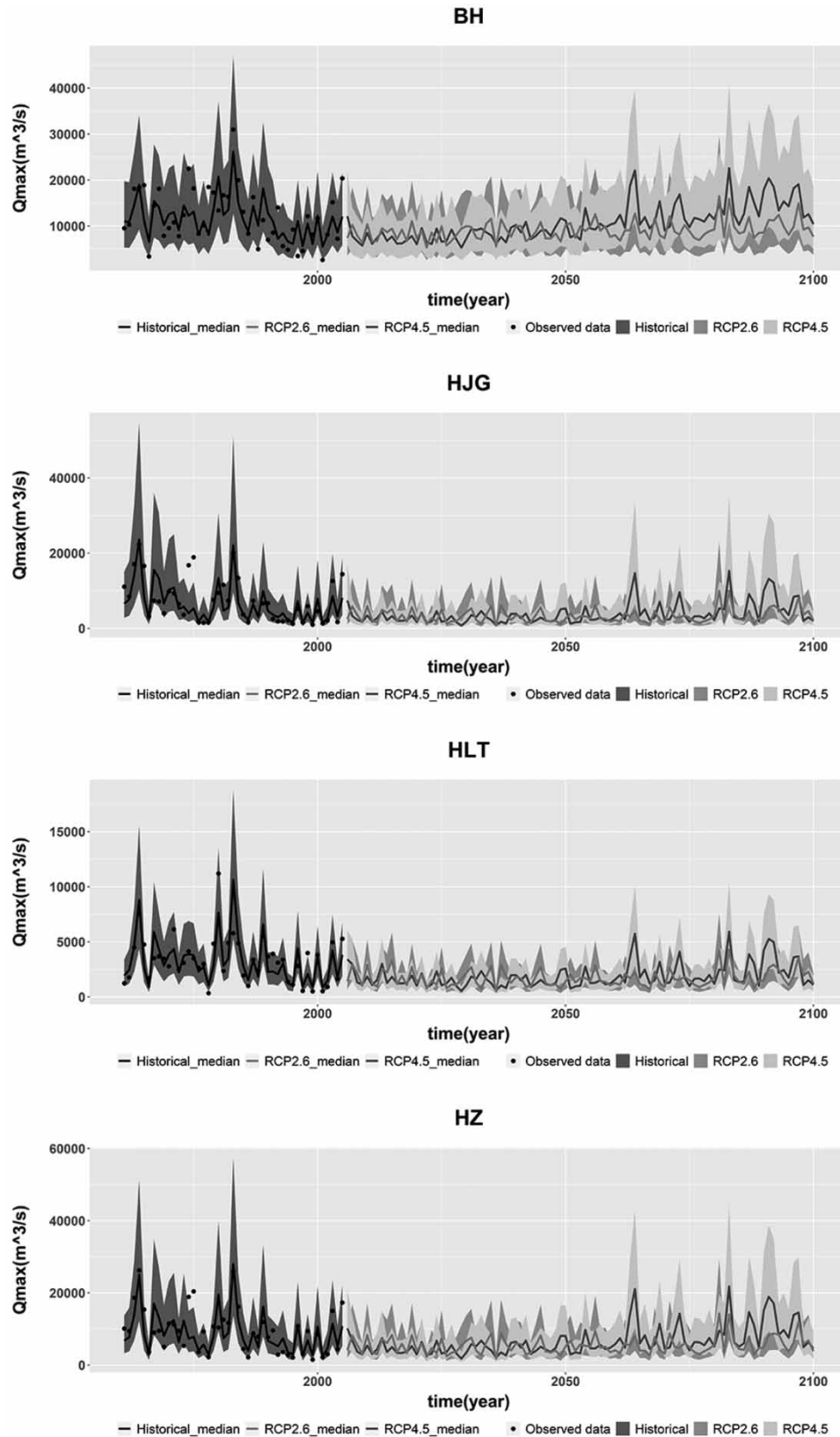


Figure 10 | Changes of the AMS projected in the future under the two RCP2.6 and RCP4.5 scenarios.

change causes further increase of flood over time. The flood risk is expected to increase in the future in the HJR Basin due to climate change, while changes in hydrological engineering and flood management are not considered. Therefore, the flood control standard and water resource allocation need to be upgraded, which is critical to multiple decision-makers in disaster risk reduction.

5. CONCLUSIONS

Due to the growing impacts of climate warming and human activities on flood regimes, the stationarity assumption of the AMS may be invalid. Evaluating flood frequency under nonstationarity is important to understand the changes in flood regimes and their physical mechanisms, which is critical to water resource management authorities in disaster risk reduction. In this paper, three kinds of models including a stationary model, nonstationary models with time and physically based factors as predictors were developed to account for the nonstationarity presented in the AMS and reveal the changing characteristics of flood regimes in the HJR Basin, as well as the projection of the AMS under the RCP2.6 and RCP4.5 scenarios. The conclusions can be summarized as below:

- The results of the three models show that for the designed flood discharge with a return period of 20 years, the variations obtained by nonstationary model 2 with physically based variables are dramatic, when compared with that obtained by stationary model 0 and nonstationary model 1 with time. The designed flood discharge by models 0 and 1 either over- or under-estimate the real AMS and, therefore, may provide misleading results for the hydraulic design. In addition, according to the AIC values, nonstationary model 2 is better than stationary model 0. Model 2-based estimated AMS can capture the impact of climate change and human activities on flood process and can provide technically reasonably designed flood discharge. These results are evidence that the assumption of stationarity in the AMS series over the HJR Basin is violated and traditional hydrological frequency analysis methods based on the stationarity assumption may lead us to assume greater risks in hydraulic design than intended.
- The periods (e.g., the early 1970 and 1990s) of sudden drops of estimated quantiles of the AMS have been identified at the four stations in the HJR Basin. These time points are in line with the completion time of water reservoirs upstream of the stations. Besides, the time points (e.g., 1980 and 1983) of peaks of estimated quantiles can also be identified. Analysis of the occurrence of precipitation extremes matches with the occurrence of the peaks of estimated quantiles, implying an influence of changes in precipitation extremes on the AMS in the HJR Basin. The detailed information of the change of AMS series can be better described by the physically based nonstationary model using climatic and anthropogenic factors as the explanatory variables in comparison with the nonstationary model with time as the covariates and the stationary model, showing the feasibility and applicability of physically based nonstationary models in modeling flood behavior and supporting the use of physically based nonstationary models.
- The climatic factors (e.g., precipitation and temperature), as explanatory variables in the nonstationary model derived from GCMs based on various climate scenarios, can produce a long-term prediction for the flood events. According to the results of this investigation, the AMS over the HJR Basin is characterized by increasing trend during 2051–2100, implying that the risk of flood is likely to increase over the HJR Basin without the consideration of changes in hydrological engineering and flood management. This study suggests that the flood control standard and water resource allocation in the HJR Basin need to be upgraded and some measures should be taken by multiple decision-makers to mitigate the potential risks posed to this region.

ACKNOWLEDGEMENTS

This work was financially supported by the Natural Science Foundation of Hebei Province of China (Grant No. E2020402057), the Belt and Road Special Foundation of the State Key Laboratory of Hydrology-Water Resources and Hydraulic Engineering (Grant Nos 2020491111 and 2019490911), the Science and Technology Research and Development Program of Handan, China (Grant No. 19422303008-73) and the Innovation Foundation of Hebei University of Engineering. The daily precipitation and temperature observations in the Hanjiang River Basin used in this study were provided by the China Meteorological Administration and the National Climate Center. They are highly appreciated. The comments and suggestions from an editor and three anonymous reviewers are gratefully acknowledged.

AUTHOR CONTRIBUTION

W.H. conceptualized the study; prepared the methodology; did formal analysis; and visualized, validated and wrote the original draft. Q.S. collected the resources, validated the study, wrote the review and edited the original draft. P.W. investigated the study and collected the resources. C.Z. validated the study. X.C. collected the resources and R.C. collected the resources and conceptualized the study.

DECLARATION OF COMPETING INTERESTS

The authors declare that they have no known competing financial interests or personal relationships that could have appeared to influence the work reported in this paper.

DATA AVAILABILITY STATEMENT

All relevant data are available from <http://climate-scenarios.canada.ca/?page=pred-canesm2>.

REFERENCES

- Akaike, H. 1974 A new look at the statistical model identification. *IEEE Transactions on Automatic Control* **19**, 716–723.
- Apurv, T., Mehrotra, R., Sharma, A., Goyal, M. K. & Dutta, S. 2015 Impact of climate change on floods in the Brahmaputra basin using CMIP5 decadal predictions. *Journal of Hydrology* **527**, 281–291.
- Buuren, S. V. & Fredriks, M. 2001 Worm plot: a simple diagnostics device for modeling growth reference curves. *Statistical in Medicine* **20**, 1259–1277.
- Chen, Y. D., Zhang, Q., Xu, C. Y., Yang, T., Chen, X. H. & Jiang, T. 2009 Change-point alterations of extreme water levels and underlying causes in the Pearl River Delta, China. *River Research and Applications* **25**, 1153–1168.
- Chen, X. C., Zhang, L. P., Shan, L. J., Yang, W. & Xu, X. 2015 Joint distribution of the extreme rainfall and flood for the upper-middle reaches of the Hanjiang River based on Copula function. *Resources and Environment in the Yangtze Basin* **24**, 1425–1433.
- Cunderlik, J. M. & Ouada, T. B. 2006 Regional flood-duration–frequency modeling in the changing environment. *Journal of Hydrology* **318**, 276–291.
- Dagnenet, F. M. & Markus, D. 2018 Analyzing the future climate change of Upper Blue Nile River basin using statistical downscaling techniques. *Hydrology and Earth System Sciences* **22**, 2391–2408.
- Donat, M. G., Lowry, A. L., Alexander, L. V., O’gorman, P. A. & Maher, N. 2016 More extreme precipitation in the world’s dry and wet regions. *Nature Climate Change* **6**, 508–513.
- Du, J. K., Qian, L., Rui, H. Y., Zuo, T. H., Zheng, D. P., Xu, Y. P. & Xu, C. Y. 2012 Assessing the effects of urbanization on annual runoff and flood events using an integrated hydrological modeling system for Qinhuai River basin, China. *Journal of Hydrology* **464–465**, 127–139.
- Eilers, P. H. C. & Marx, B. D. 1996 Flexible smoothing with B-splines and penalties (with comments and rejoinder). *Statistical Science* **11**, 89–121.
- Fang, J., Du, J., W, X. U., Shi, P. J. & Kong, F. 2014 Advances in the study of climate change impacts on flood disaster. *Advances in Earth Science* **29**, 1085–1093.
- Filliben, J. 1975 The probability plot correlation coefficient test for normality. *Technometrics* **17**, 111–117.
- Galloway, G. E. 2011 If stationarity is dead, what do we do now? *Journal of American Water Resources Association* **47**, 364–371.
- Gu, X. H., Zhang, Q., Singh, V. P., Chen, X. & Liu, L. 2016 Nonstationarity in the occurrence rate of floods in the Tarim River basin, China, and related impacts of climate indices. *Global and Planetary Change* **142**, 1–13.
- Guo, J., Guo, S. L., Zhang, J., Chen, H. & Chen, G. Y. 2009 Prediction of rainfall and runoff changes in the Hanjiang basin. *Journal of China Hydrology* **29**, 18–22.
- Hamed, K. H. & Rao, A. R. 1998 A modified Mann-Kendall trend test for autocorrelated data. *Journal of Hydrology* **204**, 182–196.
- Hannaford, J. & Marsh, T. J. 2008 High-flow and flood trends in a network of undisturbed catchments in the UK. *International Journal of Climatology* **28**, 1325–1338.
- Hao, W. L., Hao, Z. C., Yuan, F. F., Ju, Q. & Hao, J. 2019a Regional frequency analysis of precipitation extremes and its spatio-temporal patterns in the Hanjiang River Basin, China. *Atmosphere* **10**, 130. doi:10.3390/atmos10030130.
- Hao, W. L., Shao, Q. X., Hao, Z. C., Ju, Q., Baima, W. & Zhang, D. W. 2019b Non-stationary modelling of extreme precipitation by climate indices during rainy season in Hanjiang River Basin, China. *International Journal of Climatology* **39**, 4154–4169.
- He, X. H., Weng, C. H., Zhang, X. F., Du, Z. D. & Zhang, J. 2011 Research on polder flood control regulation of Dongjing Branch of Hanjiang River. *Yangtze River* **42**, 23–26.
- Hessami, M., Gachon, P., Quarda, T. & St-Hilaire, A. 2007 Automated regression-based statistical downscaling tool. *Environmental Modelling & Software* **23**, 813–834.
- Hundecha, Y. & Bardossy, A. 2008 Statistical downscaling of extremes of daily precipitation and temperature and construction of their future scenarios. *International Journal of Climatology* **28**, 589–610.
- Jin, W. H. 1986 Analysis of ‘81.8’ flood in Hanzhong and discussion on flood control. *Journal of Shanxi Water Resources* **3**, 29–38.

- Li, J. & Barker, H. W. 2005 A radiation algorithm with correlated k-distribution. Part I: local thermal equilibrium. *Journal of Atmospheric Science* **62**, 286–309.
- Li, J. Z. & Tan, S. M. 2015 Nonstationary flood frequency analysis for annual flood peak series, adopting climate indices and check dam index as covariates. *Water Resources Management* **29**, 5533–5550.
- Liu, S. Y., Huang, S. Z., Huang, Q., Xie, Y. Y. & Leng, G. Y. 2017 Identification of the non-stationarity of extreme precipitation events and correlations with large-scale ocean-atmospheric circulation patterns: a case study in the Wei River Basin, China. *Journal of Hydrology* **548**, 184–195.
- Liu, W. L., Xiong, H. L., Liu, L. N., Zhu, S. N. & Chen, X. 2019 Estimate of the climate change in Ganjiang River Basin using SDSM method and CMIP5. *Research of Soil and Water Conservation* **26**, 145–152.
- López, J. & Francés, F. 2013 Non-stationary flood frequency analysis in continental Spanish rivers, using climate and reservoir indices as external covariates. *Hydrology & Earth System Sciences* **17**, 3189–3203.
- Luo, N., Guo, Y., Gao, Z. B., Chen, K. X. & Chou, J. M. 2020 Assessment of CMIP6 and CMIP5 model performance for extreme temperature in China. *Atmospheric and Oceanic Science Letters* **6**, 589–597.
- Mallakpour, I. & Villarini, G. 2015 The changing nature of flooding across the central United States. *Nature Climate Change* **5**, 250–254.
- Mekonnen, D. F. & Disse, M. 2018 Analyzing the future climate change of Upper Blue Nile River basin using statistical downscaling techniques. *Hydrology and Earth System Sciences* **22**, 2391–2408.
- Min, S. K., Zhang, X. & Zwiers, F. W. 2011 Human contribution to more-intense precipitation extremes. *Nature* **470**, 378–381.
- Mullan, D., Chen, J. & Zhang, X. J. 2016 Validation of non-stationary precipitation series for site-specific impact assessment: comparison of two statistical downscaling techniques. *Climate Dynamics* **46**, 967–986.
- Nie, X. & Ding, L. L. 2017 Response of future water resources to climate change in the upper reaches of the Hanjiang Basin. *Journal of Anhui Agriculture* **45**, 58–60.
- Olang, L. O. & Furst, J. 2011 Effects of land cover change on flood peak discharges and runoff volumes: model estimates for the Nyando River Basin, Kenya. *Hydrological Processes* **25**, 80–89.
- Panagoulia, D., Economou, P. & Caroni, C. 2014 Stationary and nonstationary generalized extreme value modelling of extreme precipitation over a mountainous area under climate change. *Environmetrics* **25**, 29–43.
- Petrow, T. & Merz, B. 2009 Trends in flood magnitude, frequency and seasonality in Germany in the period 1951–2002. *Journal of Hydrology* **371**, 129–141.
- Qin, L. X. 1991 Discussion on regional heavy rain in the area of Hanzhong of Hanjiang River basin. *Journal of Shaanxi Meteorology* **6**, 10–12, 19.
- Qiu, B., Jiang, J. H., Sun, Z. D. & Wang, J. 2010 Analysis of trends in future temperature and precipitation in the Bosten Lake Bas in based on a statistical downscaling model. *Resources Science* **32**, 1133–1140.
- Rigby, R. A. & Stasinopoulos, D. M. 2005 Generalized additive models for location, scale and shape (with discussion). *Applied Statistics* **54**, 507–554.
- Shi, Z. H., Cai, C. F. & Ding, S. W. 2002 Research on nitrogen and phosphorus load of agricultural non-point sources in middle and lower reaches of Hanjiang River based on GIS. *Acta Scientiae Circumstantiae* **22**, 473–477.
- Tao, X. E., Chen, H. & Xu, C. Y. 2015 Characteristics of drought variations in Hanjiang Basin in 1961–2014 based on SPI/SPEI. *Journal of Water Resources Research* **4**, 404–415.
- Thiessen, A. H. 1911 Precipitation for large areas. *Monthly Weather Review* **39**, 1082–1084.
- Trenberth, K. E. 2011 Changes in precipitation with climate change. *Climate Research* **47**, 123–138.
- Velautham, D., Pradeep, M. & Lo Edmond, Y. M. 2017 A comparative frequency analysis of maximum daily rainfall for a SE Asian Region under current and future climate conditions. *Advances in Meteorology* **2017**, 1–16.
- Villarini, G., James, A. S., Francesco, S., Bales, J. D., Bates, P. D. & Krajewski, W. F. 2009a Flood frequency analysis for nonstationary annual peak records in an urban drainage basin. *Advances in Water Resources* **32**, 1255–1266.
- Villarini, G., Serinaldi, F., Smith, G. A. & Krajewski, W. 2009b On the stationarity of annual flood peaks in the continental United States during the 20th century. *Water Resources Research* **45**, 2263–2289.
- Villarini, G., Smith, G. A. & Napolitano, F. 2010 Nonstationary modeling of a long record of rainfall and temperature over Rome. *Advances in Water Resources* **33**, 1256–1267.
- Von Salzen, K., Mcfarlane, N. A. & Lazare, M. 2005 The role of shallow convection in the water and energy cycles of the atmosphere. *Climate Dynamics* **25**, 671–688.
- Wang, X. X., Wu, M. F., Lv, J. J. & Al, E. 2007 Analysis of a flood-causing heavy rainstorm in 2005 in Weihe and Hanjiang Valley. *Journal of Catastrophology* **22**, 68–71.
- Wang, W. G., Xing, W. Q., Shao, Q. X., Yu, Z. B., Peng, S. Z., Yang, T., Yong, B., Taylor, J. & Singh, V. P. 2013 Changes in reference evapotranspiration across the Tibetan Plateau: observations and future projections based on statistical downscaling. *Journal of Geophysical Research: Atmospheres* **118**, 4049–4068.
- Wang, J., Xu, Y. P., Wang, Y. F., Yuan, J., Wang, Q. & Xiang, J. 2019 Non-stationarity analysis of extreme water level in response to climate change and urbanization in the Taihu Basin, China. *Stochastic Environmental Research and Risk Assessment* **33**, 891–904.
- Wilby, R. L., Dawson, C. W. & Barrow, E. M. 2002 SDSM – a decision support tool for the assessment of regional climate change impacts. *Environmental Modelling and Software* **17**, 145–157.

- Wu, Y. T. & Polvani, L. M. 2017 Recent trends in extreme precipitation and temperature over southeastern South America: the dominant role of stratospheric ozone depletion in the CESM large ensemble. *Journal of Climate* **30**, 6433–6441.
- Wu, Z. N., Liu, S. F. & Wang, H. L. 2021 Calculation method of short-duration rainstorm intensity formula considering nonstationarity of rainfall series: impacts on the simulation of urban drainage system. *Journal of Water and Climate Change* **12**, 3464–3480.
- Xiao, Y., Du, L. M. & Ren, Y. J. 2013 Study on the relationship between typical drought/flood years in autumn flood season in Hanjiang River basin and preceding sea surface temperature. *Torrential Rain Disasters* **32**, 182–187.
- Xu, S. D. & Huang, W. R. 2011 Estimating extreme water levels with long-term data by GEV distribution at Wusong station near Shanghai city in Yangtze Estuary. *Ocean Engineering* **38**, 468–478.
- Yang, W., Zhang, L. P., Shan, L. J., Chen, X. C. & Yang, Y. R. 2015 Spatiotemporal distribution features of extreme hydrological events in the Hanjiang River Basin. *Progressus Inquisitiones De Mutatione Climatis* **11**, 15–21.
- Ye, X. C., Zhang, Q., Liu, J., Li, X. H. & Xu, C. Y. 2013 Distinguishing the relative impacts of climate change and human activities on variation of streamflow in the Poyang Lake catchment, China. *Journal of Hydrology* **494**, 83–95.
- Yin, S. Y. & Huang, C. C. 2012 Precipitation change and occurrence of rainstorms and floods in upper reaches of Hanjiang River during last 50 years. *Bulletin of Soil and Water Conservation* **32**, 19–25.
- Yue, S. & Wang, C. Y. 2004 The Mann-Kendall test modified by effective sample size to detect trend in serially correlated hydrological series. *Water Resources Management* **18**, 201–218.
- Zhai, P. M., Zhang, X. B., Wan, H. & Pan, X. H. 2005 Trends in total precipitation and frequency of daily precipitation extremes over China. *Journal of Climate* **18**, 1096–1108.
- Zhang, Q., Gu, X. H., Singh, V. P., Xiao, M. Z. & Xu, C. Y. 2014 Stationarity of annual flood peaks during 1951–2010 in the Pearl River basin, China. *Journal of Hydrology* **519**, 3263–3274.
- Zhang, D. D., Yan, D. H. & Wang, Y. C. 2015a GAMLSS-based nonstationary modeling of extreme precipitation in Beijing–Tianjin–Hebei region of China. *Nature Hazards* **77**, 1037–1053.
- Zhang, Q., Gu, X. H. & Villarini, G. 2015b Evaluation of flood frequency under non-stationarity resulting from climate indices and reservoir indices in the East River basin, China. *Journal of Hydrology* **527**, 565–575.
- Zhao, F. F. & Xu, Z. X. 2007 Comparative analysis on downscaled climate scenarios for headwater catchment of Yellow River using SDS and delta methods. *Acta Meteorologica Sinica* **65**, 653–662.
- Zhou, Y., Zhang, Q., Li, K. & Chen, X. 2012 Hydrological effects of water reservoirs on hydrological processes in the East River (China) basin: complexity evaluations based on the multi-scale entropy analysis. *Hydrological Processes* **26**, 3253–3262.
- Zhou, F., Xu, Y., Chen, Y., Xu, C., Gao, Y. & Du, J. 2013 Hydrological response to urbanization at different spatio-temporal scales simulated by coupling of CLUE-S and the SWAT model in the Yangtze River Delta region. *Journal of Hydrology* **485**, 113–125.
- Zhu, Y. P., Zang, H. P., Chen, L. & Zhao, J. F. 2008 Influence of the south-north water diversion project and the mitigation projects on the water quality of Han river. *Science of the Total Environment* **406**, 57–68.

First received 7 October 2021; accepted in revised form 19 February 2022. Available online 3 March 2022